PROCEEDINGS OF SCIENCE

The QCD phase diagram at finite temperature and density - a lattice perspective

A. Pásztor[a,b,*]

[a] *Institute for Theoretical Physics, ELTE Eötvös Loránd University, Pázmány P. sétány 1/A, H-1117 Budapest, Hungary*

[b] *HUN-REN-ELTE Theoretical Physics Research Group, Pázmány Péter sétány 1/A,1117 Budapest, Hungary*

E-mail: apasztor@bodri.elte.hu

I briefly review our current understanding of the phase diagram of strongly interacting (QCD) matter in the temperature-baryochemical potential (or baryon density) plane. I discuss properties of the chiral/deconfinement transition of QCD. I focus on results from first-principles lattice QCD simulations. I also briefly mention connections with other approaches, such as heavy ion collision experiments. I also briefly discuss the chiral transition as a function of the quark masses and it is related to thermodynamics at non-zero chemical potential.

The 40th International Symposium on Lattice Field Theory (Lattice 2023)
July 31st - August 4th, 2023
Fermi National Accelerator Laboratory

*Speaker

PoS(LATTICE2023)108

1. Introduction

The study of strongly interacting matter under extreme conditions is an active field of research, with a long history: First speculations the behavior of strongly interacting matter at high temperatures go back to Pomeranchuk in the 1950s. Modern lattice field theory techniques allow for a quantitative study of the thermodynamics of strongly interacting matter from first principles, i.e., starting from the equations of Quantum Chromodynamics (QCD), the fundamental theory governing the storng interactions. Today we know that at large enough temperatures, a form of matter called the quark-gluon plasma (QGP) is created. This strongly interacting liquid is the first form of condensed matter that appeared in the early history of our Universe. The transition from hadronic matter (where quarks and gluons are confined) to the QGP is of particular interest. At the energy scales where the transition happens, QCD is strongly coupled, which necessitates a fully non-perturbative treatment, which the lattice provides. Among other things, we known from lattice simulations that the transition in the kind of conditions that were present in the early universe, i.e. a very small, almost zero quark densities, the transition between hadronic matter and QGP is a smooth crossover [1]. Some aspects of the transition at zero density, such as the dependence of the order of the transition on the quark masses - however - remain unresolved.

Much lower temperatures and significantly larger quark (or baryon) densities, up to several times the density of atomic nuclei, are likely found in the cores of neutron stars: the most dense objects known in Nature. Mergers of neutron stars probe a slightly hotter, but still very dense part of the phase diagram. Relativistic heavy ion collisions can be used to experimentally interpolate between these two regimes: high energy collisions probe hot but not baryon dense matter, similar to the conditions in the Early Universe. Lowering the collision energy, the matter created in the collision becomes denser and colder, getting closer to the conditions found in neutron star mergers. At the larger baryon densities (or baryochemical potentials μ_B) achieved in these lower collision energy experiments, many model calculations predict a critical endpoint [2–4], where the crossover transition line turns into a firs-order transition line on the phase diagram in the temperature (T)-baryochemical potential(μ_B) plane. Locating this conjectured critical endpoint is the purpose of current as well as future heavy ion collision experiments. Unfortunately, a complex action (or sign) problem [5] makes it very difficult to extract information on the thermodynamics of QCD at non-zero μ_B from first-principle lattice simulations. Nevertheless, there are indirect ways of obtaining information on the phase diagram at non-zero (but small enough) densities (or chemical potentials). Such indirect methods have led to significant progress in our understanding of QCD matter in recent years.

In this review I present recent progress on our knowledge of QCD thermodynamics at zero and small baryochemical potentials. The structure of this review is as follows: First, I review thermodynamics at zero baryochemical potential. I will discuss aspects of the chiral transition, the nature of the chiral transition as a function of the quark masses - the so-called Columbia plot and aspects of the $U(1)_A$ anomaly. Second, I will review thermodynamics at non-zero baryochemical potential. I will discuss the sign problem, results from analytic continuation techniques the Taylor series in the baryochemical potential μ_B around $\mu_B = 0$ and its resummations, and recent developments on reweighting techniques. Note that in this review I ignore other possible variables of interest, such as a non-zero isospin density [6], magnetic field [7, 8], or strangeness density [9, 10].

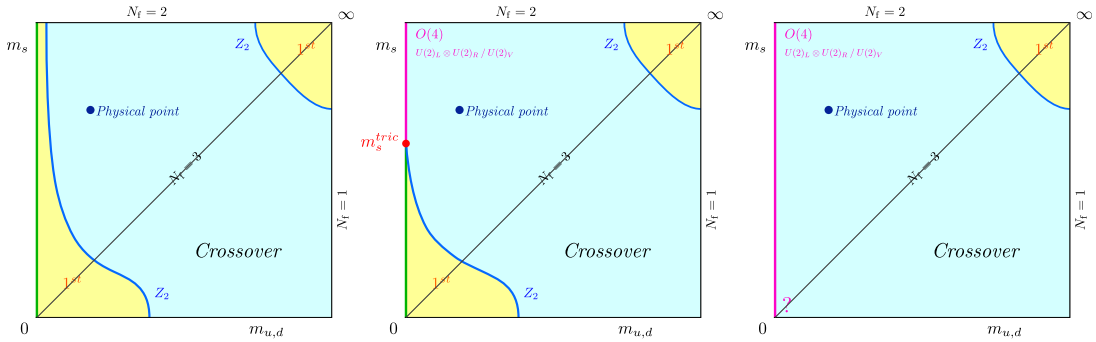

Figure 1: Three different scenarios for the Columbia plot (see main text). Sketches taken from Ref. [11].

2. Aspects of the chiral transition and the chiral limit

In the limit of N_f quark masses going to zero, QCD has an $SU(N_f)_L \times SU(N_f)_R$ global symmetry, called chiral symmetry. It is generally believed that in this limit, the QCD transition is not a crossover anymore, but a genuine phase transition, where chiral symmetry, that is spontaneously broken to its $SU(N_f)_V$ subgroup at low temperatures, is restored. The order parameter for this phase transition in the chiral limit is called the chiral condensate. The bare chiral condensate and the chiral susceptibility are defined by differentiating the free energy with the light quark mass, which we assume to be the same for the two light flavours $m_{ud} = m_u = m_d$, giving:

$$\langle \bar{\psi}\psi \rangle = \frac{T}{V} \frac{\partial \log Z}{\partial m_{ud}}, \qquad \chi_{\rm ch} = \frac{\rm T}{\rm V} \frac{\partial^2 \log \rm Z}{\partial \rm m_{ud}^2}. \tag{1}$$

The condensate and the susceptibility have an additive and multiplicative divergence, which has to be renormalized. One way to remove the additive divergence is by subtracting the zero temperature contribution, and one way to remove the multiplicative divergence is by multiplying with a quark mass. This leads to one possible definition of a renormalized condensate and susceptibility:

$$\langle \bar{\psi}\psi \rangle^R = \frac{m_{ud}}{f_\pi^4} \left[\langle \bar{\psi}\psi \rangle_0 - \langle \bar{\psi}\psi \rangle_T \right], \qquad \chi^{\rm R}_{\bar{\psi}\psi} = \frac{\rm m_{ud}}{\rm f_\pi^4} \left[\chi_0 - \chi_{\rm T} \right]. \tag{2}$$

In the limit of zero quark mass, there is no additive renormalization, due to chiral symmetry. In this limit the chiral condensate is an order parameter for chiral symmetry breaking/restoration: it is zero when chiral symmetry is restored at high temperatures, and non-zero when chiral symmetry is broken at low temperatures. For a finite quark mass, there is no exact chiral symmetry and thus no exact order parameter. Still, the inflection point of the condensate or the peak position of the susceptibility can be used to define the crossover temperature. Similarly, finite volume scaling of the susceptibility can be used to study the order of the transition. While it is very well established that the chiral transition is a crossover for physical quark masses [1], how this situation change for smaller-than-physical masses is not known.

2.1 The Columbia plot

The nature of the QCD transition with $N_f = 2 + 1$ quark flavours as a function of the quark masses is summarised in the so-called Columbia plot: the vertical axis is the strange quark mass

m_s, while the horizontal axis is the common light quark mass $m_{ud} = m_u = m_d$. Several scenarios for the Columbia plot are sketch in Fig. 1. If both the light quark mass m_{ud} and the strange quark mass m_s are taken to infinity, we arrive at the quenched limit: pure $SU(3)$ gauge theory. In this limit, the transition is first order [12], characterized by the spontaneous breaking of the Z_3 center symmetry [13]. Locating the large values of the quark masses in the top right corner of the Columbia plot where the transition turns to a crossover at a critical line of the 3D Ising universality class is subject to ongoing research [14]. The main difficulty in locating it is in the cut-off effects: The small Compton-wavelength of heavy quarks requires requires small lattice spacings for a reliable continuum extrapolation.

In the opposite limit of light (or zero) quark masses, chiral symmetry emerges. The two-flavor chiral limit $m_{ud} \to 0$ corresponds to the left edge of the Columbia plot, while the three-flavor chiral limit $m_{ud} = m_s \to 0$ corresponds to the bottom left corner. In the N_f-flavor chiral limit, there is a global $SU(N_f)_L \times SU(N_f)_R$ chiral symmetry, which is broken spontaneously to the $SU(N_f)_V$ subgroup, with the corresponding Goldstone-bosons being the $N_f^2 - 1$ pions. The order parameter for this symmetry breaking is the chiral condensate. In addition, the anomalously broken $U(1)_A$ symmetry also plays an important role. Thinking on the Columbia plot is heavily influenced by the seminal work in Ref. [15], that presents a perturbative renormalization group analysis (using the ϵ expansion) of the possible existence of renormalization group (RG) fixed points with the given symmetry breaking pattern. They find that the existence of the corresponding RG fixed points depends on the effective restoration of the anomaly, i.e., whether anomaly- induced terms are present in the Landau-Ginzburg effective action, or not. In the case an effectively restored anomaly, no RG fixed point was found for the $N_f = 2$ or $N_f = 3$ chiral limit, implying that the transition cannot be second order. For the case with no effective anomaly restoration, there was no fixed point found for the $N_f = 3$ case, while the $N_f = 2$ case corresponds to the three-dimensional $O(4)$ universality class. Futhermore, Ref. [16] argues that the transition in the $N_f = 2$ chiral limit can only be continuous if the effective breaking of $U(1)_A$ is sufficiently large. In summary, the standard lore is that the scenario on the left panel of Fig. 1. corresponds to a case with an effectively restored anomaly, while the scenario in the middle panel corresponds to a case with a broken anomaly. Recently, in Ref. [17] a different analysis was presented, with a functional renormalization group approach, where a fixed point was found for the $N_f = 3$ case. One important feature, in which Ref. [17] differs from earlier treatments is a larger set of couplings on which the RG flows are analyzed. If this new RG fixed point (or new universality class) indeed exists, that leaves open the possibility of the scenario for the Columbia plot which is shown in the right panel of Fig. 1. In this particular case, there would no first order region in the bottom left corner of the Columbia plot and the transition could be second order in both the $N_f = 2$ and $N_f = 3$ chiral limit.

The left edge of the Columbia plot, i.e., the $N_f = 2$ chiral limit has also been studied with lattice simulations. The phase transition temperature in the chiral limit was estimated to be around 130MeV, based on simulations with HISQ fermions [18]. Later, the transition was also studied with a different discretization, twisted mass Wilson fermions in Ref. [19], with a compatible estimate for the transition temperature in the two-flavour chiral limit. The available simulations cannot clearly identify the order of the transition in the two-flavor chiral limit: while the data are consistent with $O(4)$ scaling, Ising criticality with a small critical value for the quark mass (corresponding to the first order scenario in the chiral limit) cannot be rigorously ruled out.

Direct lattice QCD treatments of the bottom left corner of the Columbia plot are the most challenging, due to the large cut-off effects present for observables related to chiral symmetry. For coarse (unimproved) staggered lattices, a first order region can be found on the bottom left corner of the Columbia plot. Repeating this first order region search for smaller lattice spacings with the unimproved staggered action, there is no evidence that this first order region survives in the continuum limit [11]. This might lead one to suspect the right panel of Fig. 1. to be correct. However, studies based on unimproved staggered fermions cannot be conclusive, due to potentially severe cut-off effects. Ideally, one should aim to study the issue with a chiral discretization, such as overlap or domain wall fermions. Recent preliminary results with Möbius domain-wall fermions suggest that at least for the case of the light quark having physical masses and $m_{ud} = m_s$, the transition is still a crossover [20]. A recent lattice study with HISQ fermions with a fixed number of time-slices again does not find a first order region [21] in the lower left corner of the Columbia plot. This is again not conclusive as staggered fermions with a fixed lattice spacing do not possess the full chiral symmetry, but it is an indication that if a first order region exists, it is practically very hard to find. Using a non-lattice approach, a recent calculation using truncated Dyson-Schwinger equations [22] also does not find a first order region in the three flavour chiral limit.

In summary, the long-standing standard scenarios in the left and middle panels of Fig. 1 have come under question in recent works. To finally resolve the important open issue of the Columbia plot, it is important both to establish or rule out the existence of a new universality class for the three-flavour chiral limit, and to advance lattice simulations with chirally symmetric fermions, such that the chiral limit can be sufficiently approached in full QCD.

2.2 Aspects of the $U(1)_A$ anomaly at high temperature

It is clear from the previous discussion that the fate of the anomalous $U(1)_A$ symmetry plays a key role in the chiral limit. The central idea here as an effective restoration of $U(1)_A$ at high temperatures. If such an effective restoration takes place, certain quantities which should be zero for an intact $U(1)_A$ symmetry, but are non-zero at zero temperature, become zero at high temperatures (in the chiral limit). An often studied example is the different between the susceptibility for the π and δ mesons, which can be written in terms of the spectral density $\rho(\lambda)$ of the Dirac operator as:

$$\chi_\pi - \chi_\delta = \int d\lambda \frac{m^2}{(m^2+\lambda^2)^2}. \tag{3}$$

This is to be contrasted with the chiral condesate, which is written in terms the spectral density as:

$$\langle \bar{\psi}\psi \rangle = \int d\lambda \frac{m}{m^2+\lambda^2}. \tag{4}$$

Due to the kernel in the above integral formulae, both are dominated by small eigenvalues of the Dirac operator in the chiral limit. It is, however, possible, to have a chiral limit where at large temperatures we have $\langle \bar{\psi}\psi \rangle = 0$ but $\langle \bar{\psi}\psi \rangle \neq 0$. This would be an example of chiral symmetry restoration without effective restoration of $U(1)_A$. If, on the other hand, in the chiral limit $\langle \bar{\psi}\psi \rangle = 0$ and $\langle \bar{\psi}\psi \rangle = 0$, we talk about chiral symmetry restoration being accompanied by an effective restoration of $U(1)_A$. The exact behavior of low modes of the Dirac operator is key in understanding this issue. Low modes in the Dirac operator are in turn related to topolocial excitations (instantons/calorons). In

Ref. [23] it was shown that analyticity in the quark masses (due to the absence of Golstone modes at high temperature) and analyticity of the spectral density imply the effective restoration of $U(1)_A$. However, there is growing numerical evidence that the QCD spectral density develops a (singular) peak near zero at high temperatures [24–28] (with the exception of Ref. [29], where the suppression of the low mode peak could be due to the small volume used for the simulations). A simple but plausible explanation for the known features of small Dirac modes is given recently in a matrix model of high temperature instantons, introduced in Ref. [30]. The model predicts $\chi_\pi - \chi_\delta = 0$ in the three-flavour chiral limit (suggesting effective restoration), but $\chi_\pi - \chi_\delta \neq 0$ in the two-flavour chiral limit (suggesting that $U(1)_A$ remains broken).

3. Non-zero baryochemical potential

In QCD processes the net number of any quark flavour is conserved. For three flavors of quarks, this implies the existence of three conserved charges, the net number of u, d and s quarks separately: N_u, N_d and N_s. In the grand canonical ensemble, a chemical potential is coupled to each of these charges. Obviously any linear combination of the three charges is also conserved. Instead of the three quark numbers, the baryon number N_B, the electric charge N_Q and strangness N_S is often used instead. The quark chemical potentials are related to the baryon number, strangeness and electric charge chemial potentials via the charges of the different quark flavours:

$$\mu_u = \frac{1}{3}\mu_B + \frac{2}{3}\mu_Q, \qquad \mu_{\rm d} = \frac{1}{3}\mu_{\rm B} - \frac{1}{3}\mu_{\rm Q}, \qquad \mu_{\rm s} = \frac{1}{3}\mu_{\rm B} - \frac{1}{3}\mu_{\rm Q} - \mu_{\rm S}. \tag{5}$$

Generalized susceptibilities are important observables in this context. These can be defined in either the u,d,s or the B,Q,S basis as derivatives of the pressure p:

$$\chi^{uds}_{ijk} = \frac{\partial^{i+j+k}\left(p/T^4\right)}{\partial\left(\mu_u/T\right)^i \partial\left(\mu_d/T\right)^j \partial\left(\mu_s/T\right)^k} \qquad \chi^{BSQ}_{ijk} = \frac{\partial^{i+j+k}\left(p/T^4\right)}{\partial\left(\mu_B/T\right)^i \partial\left(\mu_S/T\right)^j \partial\left(\mu_Q/T\right)^k}. \tag{6}$$

The χ^{uds}_{ijk} can be obtained as linear combinations of the χ^{BSQ}_{ijk} and vice versa. When either of the i,j or k indices are zero, we omit the corresponding upper and lower indices. E.g. we define $\chi^{BS}_{ij} = \frac{\partial^{i+j}\left(p/T^4\right)}{\partial(\mu_B/T)^i \partial(\mu_S/T)^j}$ and $\chi^{B}_{i} = \frac{\partial^{i}\left(p/T^4\right)}{\partial(\mu_B/T)^i}$. All of these susceptibilities are functions of the temperature T as well as the three different chemical potentials. The susceptibilities appear in many physics applications, some of which I will discuss shortly.

Most calculations do not consider the full 4-dimensional $T - \mu_B - \mu_S - \mu_Q$space. Rather, they show observables as a function of T and μ_B only, while using extra conditions to fix the values of the other two chemical potentials. Common choices here include a zero strangeness chemical potential $\mu_S = 0$ or a zero strange quark chemical potential $\mu_s = 0$. A more realistic choice, corresponding to the initial conditions in a heavy ion collision, is strangeness neutrality, which requires a tuning of μ_S in such a way that $\chi^S_1 = 0$ is satisfied for all μ_B and T. The electric charge chemical potential is most often chosen to be zero: $\mu_Q = 0$. A more realistic choice is to tune the chemical potentials in such a way that $0.4\chi^B_1 \approx \chi^Q_1$. This is motivated by the fact that the heavy nuclei collided by experiments, such as gold or lead, has slightly more neutrons than protons in the initial state. In subsequent sections I will discuss observables as a function of μ_B, but I will also shortly state the choices made for μ_S and μ_Q for any particular calculation.

3.1 The complex action/sign problem and extrapolation methods

For three flavour of quarks on the lattice, the grand canonical partition function is written as:

$$Z = \int \mathcal{D}U \det M(U, m_u, \mu_u) \det M(U, m_u, \mu_u) \det M(U, m_u, \mu_u) e^{-S_{YM}(U)}, \tag{7}$$

where U are the usual link variables on the lattice, S_{YM} is the discretized Yang-Mills action and the three factors of $\det M$ are the quark determinants for the $u/d/s$ quarks respectively. The quark determinants depend on the quark masses and the quark chemical potentials. Eq. (7) uses a schematic notation, meaning that the details of the discretization are suppressed both in S_{YM} and the quark determinants, and staggered rooting is omitted from the formula, in the case of staggered fermions. It can be show that $\det M(U, m, \mu)^* = \det M(U, m, -\mu^*)$, where the $(\dots)^*$ denotes complex conjugation. It immediately follows that the determinant is real for a zero or purely imaginary chemical potential. If the discretization also has at least a $U(1)$ remnant of chiral symmetry, such as staggered or minimally doubled fermions, the determinant can also be shown to be positive in these cases. In other situations, the determinant can be complex, leading to the breakdown of importance sampling. The presence of the sign problem makes direct simulations at real $\mu \neq 0$ incredibly difficult. Thus, most results on QCD at non-zero density come from some kind of extrapolation, either from zero or purely imaginary chemical potentials.

The Taylor method: For simplicity, consider the case of $\mu_S = \mu_Q = 0$. The Taylor expansion of the pressure $p(T, \mu_B)$ or the baryon number susceptibility $\chi_2^B(T, \mu_B)$ can then be written as:

$$\begin{aligned} (p(T, \mu_B) - p(0, \mu_B))/T^4 &= \chi_2^B(T,0)\,(\mu_B/T)^2\,/2! \quad &&+\chi_4^B(T,0)\,(\mu_B/T)^4\,/4! + \dots \\ \chi_2^B(T, \mu_B) &= \chi_2^B(T,0) &&+\chi_4^B(T,0)\,(\mu_B/T)^2\,/2! + \dots \end{aligned} \tag{8}$$

For other choices of the chemical potentials, such as, e.g., the case of strangeness neutral matter, the Taylor coefficients can also be worked out, and they are combinations of the different $\chi_{nm}^{BS}(T,0)$ coefficients [31]. The Taylor expansion coefficients, such as $\chi_n^B(T,0)$, can be expressed as sums of products of the expectation values of products of traces of products involving the inverse Dirac operator and its derivatives with respect to the chemical potential. The standard way to evaluate these is a stochastic method, using random Gaussian sources [32]. This way, the Taylor coefficients can be evaluated using simulations at zero chemical potential. In addition to the pressure, other observables can be Taylor expanded as well. Those Taylor coefficients can also be calculated with $\mu_B = 0$ simulations. Since the Taylor coefficients allow for an extrapolation to small non-zero μ_B, this gives us a windows into hot-and-dense QCD matter.

The imaginary chemical potential method: An alternative way to extrapolate to non-zero real μ_B is to perform simulations at purely imaginary μ_B, i.e., $\mu_B^2 \leq 0$, a situation with no sign problem. If an observable is calculated for several values of $\mu_B^2 \leq 0$, one can use ansätze in μ_B^2 to extrapolate it to $\mu_B^2 > 0$. An obvious source of systematic errors here is the choice of the extrapolation ansatz, which is conceptually on a similar footing as the truncation errors in a Taylor expansion. The Taylor and imaginary chemical potential methods are obviously strongly related, as they are both based (mathematically speaking) on analytic continuation. These are the methods that gave us most of our knowledge on physics at non-zero baryochemical potential to date.

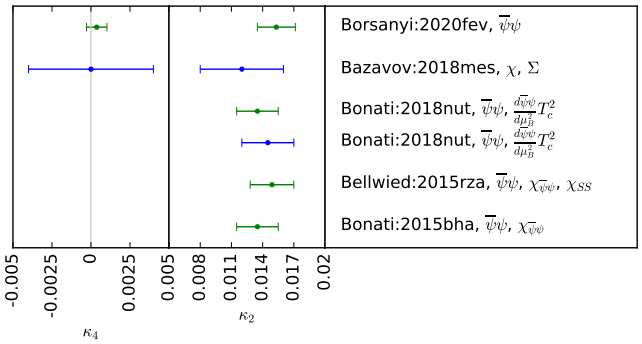

Figure 2: Taylor coefficients of the crossover line $T_c(\mu_B)$ (see equ.(9)) for strangeness neutral matter. Results from several collaborations are compared (see main text). The calculational method is color coded: green points use the imaginary chemical potential method while blue points use the Taylor method.

3.2 The phase diagram at small μ_B

The value of the crossover temperature at $\mu_B = 0$ is well established [33, 34]. A recent, precise latice QCD calculation [35], based on the chiral condensate (see eqs. (1) and (2)), gives $T_c(\mu_B = 0, LT = 4) = 158.0 \pm 0.6$MeV. At $\mu_B > 0$, the transition temperature is usually written as a Taylor expansion:

$$T_c(\mu_B)/T_c(0) = 1 - \kappa_2 \left(\mu_B/T_c(\mu_B)\right)^2 - \kappa_4 \left(\mu_B/T_c(\mu_B)\right)^4 + \ldots . \tag{9}$$

The expansion is written in terms of $\mu_B/T_c(\mu_B)$ and not μ_B due to convenience: the quark determinant on the lattice for quark flavour f only depends on the ratio μ_f/T, chemical potential-to-temperature ratios are thus the natural quantities for an expansion. Of course, the coefficients κ_2 and κ_4 can be converted to Taylor expansion coefficients in the chemical potential μ_B itself [36]. The coefficients κ_2 and κ_4 can and have been be calculated with both the Taylor or the imaginary chemical potential methods. Results with the two methods agree. For the κ_2 coefficient, calculations by the Pisa group, the Wuppertal-Budapest group and the HotQCD group are in good agreement [35, 37–40]. For the κ_4 coefficient, there are two calculations at the moment, one by the HotQCD collaboration, using the Taylor method [40], and one by the Wuppertal-Budapest collaboration, using the imaginary chemical potential method [35]. These are again in agreement. Available continuum extrapolated results for the case of strangeness neutral matter are summarized in Fig. 2. All determinations in the comparison use chiral observables to define T_c. The most precise determination of the κ_2 and κ_4 coefficients at the moment can be found in Ref. [35], giving:

$$\kappa_2 = 0.0153 \pm 0.0018, \qquad \kappa_4 = 0.00032 \pm 0.00067. \tag{10}$$

Thus, the transition line on the phase diagram at small enough μ_B is - to a very good approximation - a parabola. A joint Bayesian analysis [36] of the Taylor coefficient data of Ref. [40] and the imaginary chemical potential data of Ref. [35] suggest that the transition line can be well approximated with a parabola in μ_B (but not in $\mu_B/T_c(\mu_B)$) up to chemical potentials as high as $\mu_B \approx 600$MeV.

3.2.1 Chemical freeze-out

It is worth comparing the QCD transition line to the phenomenological chemical freeze-out line in heavy ion collisions. Chemical freeze-out is the point in the time-evolution of a heavy ion collision where non-elastic scattering rates between hadrons become slower than the expansion rate of the fireball, and hadron yields are frozen. On the phase diagram, chemical freeze-out is characterized by a curve in the $T - \mu_B$ plane. At zero baryochemical potential, the freeze-out temperature T_{ch} is expected to be close to the crossover transition [41]. This is indeed the case: T_{ch} at large collision energies (corresponding to small μ_B) approximately agrees with, or is slightly below $T_c(\mu_B = 0)$ [42–45]. On the other hand, at large μ_B, the freeze-out curve is expected to be significantly below the chiral transition line, as it is expected to approach the nuclear-liquid gas critical point [46], where there is chiral symmetry breaking and quark confinement on both sides of the transition. Where and how the deviation between the chiral transition curve and the freeze-out curve happens on the phase diagram is an important open question.

3.3 Taylor coefficients near $\mu_B = 0$ and comparisons with the hadron resonance gas

Knowing the $T_c(\mu_B)$ curve discussed previously does not automatically lead to a determination of the position of the covated critical endpoint (CEP). For that purpose, other observables have to be considered. On possibility is the study of baryon number fluctuation observables, such as $\chi_2^B(T, \mu_B)$, which should diverge at a CEP. Since they are the Taylor coefficients of $\chi_2^B(T, \mu_B)$, the higher order fluctuations at μ_B, i.e., $\chi_n^B(T, \mu_B = 0)$, could also show signs of the conjectured CEP. Since $T_c(\mu_B)$ decreases with increasing μ_B, the critical endpoint should be below the crossover temperature at $\mu_B = 0$. Thus, a way to look for signs of criticality is to study high order Taylor coefficients at $\mu_B = 0$ in the hadronic phase. A commonly used model of QCD thermodynamics in the hadronic phase is given by the hadron resonance gas model. This model approximates the QCD pressure as a sum of partial pressures for hadrons and hadron resonances, both treated as free particles. It is a simple approximation of the S-matrix formalism of statistical mechanics for the case when the scattering matrix is dominated by the production of narrow resonances [47, 48]. In the context of the CEP search, the hadron resonance gas plays a key role, as a non-critical model that describes the hadronic phase of QCD quite well. A minimal goal for criticality search could then be to establish deviations from the hadron resonance gas and full QCD data, e.g. of the coefficients $\chi_n^B(T, \mu_B = 0)$ at low temperatures.

The lattice QCD community has spent considerable effort in calculating these coefficients. The highest order coefficient available from the lattice is χ_8^B [49–53]. In Fig. 3 three different lattice QCD results are shown for the the coefficients χ_6^B and χ_8^B. The green bands are results of the HotQCD collaboration [52], using the Taylor method and a coarser lattice, with HISQ fermions [54] and 8 timeslices. The black points are results from the Wuppertal-Budapest collaboration [50], using the imaginary chemical potential method, on a finer lattice, with 4stout fermions [55] and 12 timeslices. Finally, the orange bands shows recent results from the Wuppertal-Budapest collaboration [53] in the continuum limit, using the Taylor method, but with a physical box size L that is half the value of that of the other two calculations. The continuum limit extrapolation was possible due to the introduction of the novel 4HEX discretization. In addition to the different lattice spacing and slightly different discretization (different versions of rooted staggered fermions) the HotQCD calculation

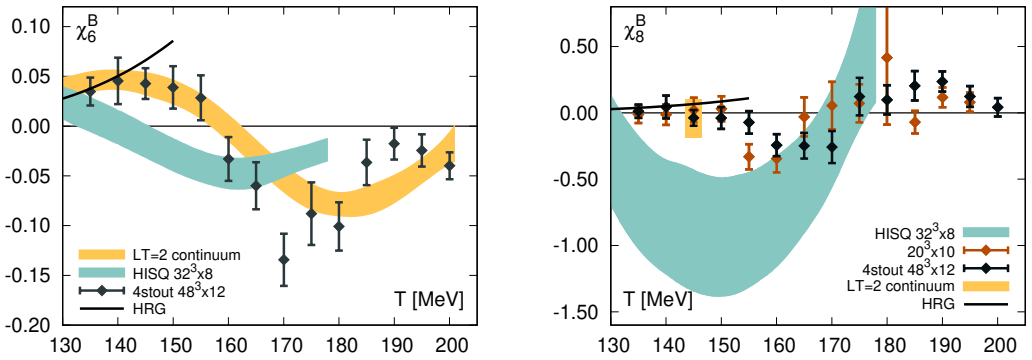

Figure 3: χ_6^B (left) and χ_8^B at $\mu_B = 0$ from different lattice QCD calculations (see main text). The solid black lines show predictons of the hadron resonance gas model.

also differs from the other two calculations in how it defines the chemical potential on the lattice. While the two 4stout and 4HEX results both use the standard exponential definition, which couples to the exact conserved charges on the lattice [56], the HISQ result uses the linear definition, which is much less understood in terms of renormalization and cut-off effects. There is a striking tension between the green bands and the other two results, which makes one conclude that the $N_\tau = 8$ HISQ results are probably effected by large cut-off effects. On the other hand, agreement between the black points and the orange bands below $T = 145$MeV indicate that in this range (which is the most relevant range for the CEP search) the finite volume effects are already negligible for the smaller volume result from Ref. [53]. The lattice results are compared with the prediction from the hadron resonance gas (HRG) model (solid black line). In regards to the comparison with the hadron resonance gas at the low temperatures relevant for the CEP search, we find that the 4stout and 4HEX results are in much better agreement with the HRG than the HISQ results. We thus can conclude that the Taylor coefficients up to 8th order are in good agreement with the HRG model for all temperatures below $T \approx 145$MeV, as long as the continuum limit is taken[1].

Let me warn the reader here, that this does not necessarily imply that the CEP does not exist. It is also a possiblity, that it exists, but its effects on coefficients up to χ_8^B are smaller than the current error bars, or that its effects are only substantial for higher order coefficients.

Finally, let me note that there have been attempts to extract the position of the leading singularity of the QCD free energy from lattice QCD data [57–60], with the hope of eventually arriving at a prediction for the critical endpoint position. Unfortunately, these calculations have all been based on lattice QCD results on coarse lattices. Considering the rather large cut-off effects at $\mu_B > 0$, which can be seen, e.g., in the green bands of Fig. 3., these works are at the moment have no solid indications for heavy ion phenomenology. They are interesting to lattice practitioners, however, as they introduce several novel methods to analyze lattice data from either the Taylor or the imaginary chemical potential methods.

[1]Since corrections to the HRG model are expected to be exponentially suppressed at small T [47] agreement for the range available on the lattice implies that χ_6^B and χ_B^8 will likely also agree with the HRG at lower temperatures.

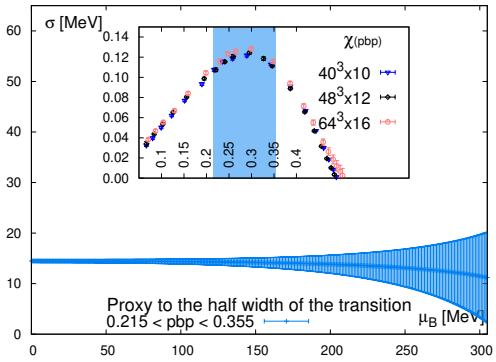

Figure 4: The width of the transition as a function μ_B, from analytic continuation from an imaginary μ_B.

3.4 The width of the transition and resummations based on shifting sigmoid functions

Since the chiral/deconfinement transition at $\mu_B = 0$ is a crossover, there is no non-analyticity in the free energy, and thus no sharp point of transition. Rather, there is an extended transition region in T, which can be characterized with a width parameter. One possible definition of such a width parameter σ is given in Ref. [35]. The definition is based on a finite difference approximation of the temperature derivative of the renormalized chiral condensate of eq. 2. When the T derivative is large at T_c, the width parameter is small so the transition is narrow. When the T derivative is small, the width parameter is large and the transition is broad. In Ref. [35], this σ width parameter was also extrapolated to real μ_B using the imaginary chemical potential method. The results are shown in Fig. 4. σ going to zero would indicate the presence of a CEP. The results show that for small μ_B the width σ is approximately constant: The transition does not get narrower below the value of $\mu_B \approx 300$MeV, where the error bars blow up, and the extrapolation becomes unpredictive.

Another way to see the approximately constant width of the crossover is through the existence of an approximate scaling variable [10, 61, 62]. The existence of this approximate scaling variable is illustrated in Fig. 5, where the baryon-density-to-chemical potential ratio $\chi_1^B/(\mu_B/T)$ is plotted as a function of T (left panel) and as a function of $T\left(1+\kappa_2\left(\frac{\mu_B}{T}\right)^2\right)$ the curvature of the transition line [2]. Thus, Figs. 4 and 5 tell the same story: the story of a crossover transition whose temperature depends on the chemical potential, but its width does not. What happens with the width of the transition at larger μ_B is an open question.

A plausible explanation for the existence of the observed approximate scaling variable can be the conjectured $O(4)$ criticality in the two-flavour chiral limit of QCD. To understand why this is the case let me note two empirical observations: i) the ratio $\chi_1^B/(\mu_B/T)$ does collapse in the new variable, while the second derivative χ_2^B does not, and ii) the renormalized chiral condensate defined in equation (2), which is made dimensionless by division with f_π^4 does collapse in the new variable but if we make it dimensionless by dividing with T^4 instead, it no longer collapses. Both of these observations are natural if the $O(4)$ universal contribution to thermal free energy is large.

[2]The numerical value of κ_2 in eq. (10) and in Fig. 5 is different, because in eq. (10), the result is quoted for strangeness neutral QCD matter, while Fig. 5 is for illustration purposes only, and uses the simpler case of zero strangeness chemical potential $\mu_S = 0$.

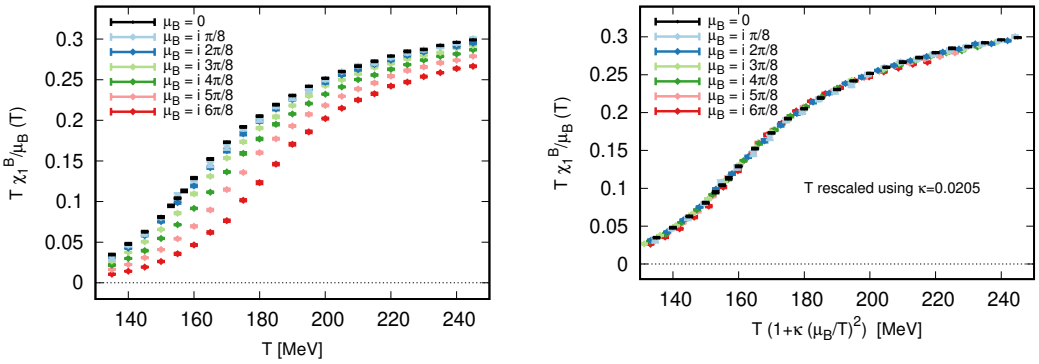

Figure 5: The ratio $\chi_1^B/\hat{\mu}_B$ as a function of the temperature T (left) and the approximate scaling variable $T(1+\kappa\hat{\mu}_B^2)$ for different values of an imaginary chemical potential-to-temperature ratio.

Using this assuption, and the universal form of the equation of state

$$p_{QCD}(T, m_{ud}, \mu_B) - p_{QCD}(0, m_{ud}, \mu_B) \sim t^{2-\alpha}\mathcal{G}\left(h/t^{\beta\delta}\right), \tag{11}$$

where α, β, δ are $O(4)$ critical exponents and $\mathcal{G}$ is the universal $O(4)$ equation of state, and the scaling variables h and t are mapped to the QCD variables approximately $h \sim m_{ud}$ and $t \sim (T - T_c^{m_{ud}\to 0})/T_c^{m_{ud}\to 0} + \kappa_2 (\mu_B/T)^2$. Simple differentiation of eq. 11 show that the observables that do collapse as a function of the approximate scaling variable ($T\chi_1^B/\mu_B$ and $\langle\bar{\psi}\psi\rangle^R$ of equ. (2)) are exactly those that only depend on the scaling variables h and t, while the observables that do not show collapse (χ_2^B and $\langle\bar{\psi}\psi\rangle^R \frac{T^4}{f_\pi^4}$) are not only dependent on h and t, but also T and μ_B separately.

The existence of an approximate scaling variable can be used to define an alternative extrapolation/resummation scheme. Technically, this is done via an implicit equation for some observable F (to be specified later):

$$\begin{aligned} F(T, \mu_B) &= F(T'(T, \mu_B), \mu_B = 0), \\ T'(T, \mu_B) &= T\left(1 + \kappa_2^F(T)\,(\mu_B/T)^2 + \kappa_4^F(T)\,(\mu_B/T)^4 + \ldots\right). \end{aligned} \tag{12}$$

These equations, together with a choice for the observable F define a resummation/extrapolation scheme. This is a systematically improvable expansion. The Taylor coefficients of the "intermediate temperature" $T'(T, \mu_B)$ are observable dependent, thus the superscipt F in the notation of κ_n^F. This is not a Taylor expansion for the observable F itself. Rather, any finite order in the Taylor expansion of $T'(T, \mu_B)$ generates an infinite number of Taylor coefficients for F. The validity of the expansion is not predicated on the existence of an approximate scaling variable, only its fast convergence: i.e., if an approximate scaling variable exists, we expect the method to converge faster. In Ref. [61] where the method was originally proposed, it was used for the case $\mu_S = \mu_Q = 0$ with the choice $F = T\chi_1^B/\mu_B$ to calculate the equation of state. Later, this resummation for the equation of state was also performed for the case of strangness neutral matter (still with $\mu_Q = 0$) in [10], with a more elaborate choice of F, which improved the convergence of the scheme at high temperatures.

One interesting application of the equation of state calculation is the calculation of isentropes: curves of constant entropy density to baryon density ratio s/n_B in the $T - \mu_B$ plane. Near the CEP, they are expected to show the phenomena of critical lensing [63, 64]: the CEP pulls the isotropes

towards itself, increasing their local density in the critical region. Fig. 6 shows preliminary results on the isentropes from the resummation/alternative expansion scheme. While the alternative scheme can reach larger values of μ_B, the qualitative conclusion from the Taylor expansion [65] and the resummation are the same: within errors, and within covered values of μ_B, there is no critical lensing. The largest density isentrope, with $s/n_B = 20$ roughly corresponds to the smallest collision energy available in the RHIC Beam Energy scan in collider mode [66, 67]. In Ref. [68], a phenomenological application of the resummation scheme of eq. (12) is presented, that shows how to incoporate the existence of a conjectured CEP in the resummation scheme. This will certainly be useful for future studies searching for the CEP.

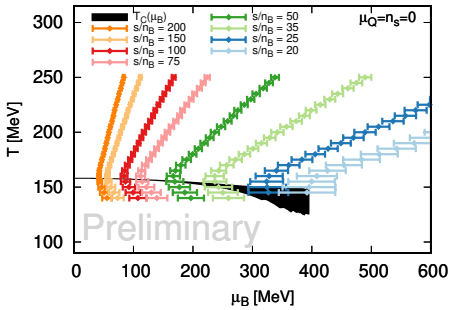

Figure 6: Isentropes of the T-μ_B plane from the alternative expansion scheme of Refs. [10, 61]

3.5 Reweighting techinques

The Taylor and imaginary chemical potential methods both require an analytic continuation, which is known to be numerically ill-posed. In order to avoid this ill-posedness, and go beyond the current reach of such methods, the development of more direct simulation methods at $\mu_B > 0$ is desirable. Reweighting techniques provide an opportunity to do exactly that. Even more importantly, such a more direct approach has the promise of generating very different data for the CEP search: data at larger real μ_B, closed to the critical endpoint we would like to locate.

Given a theory with field variables U, reweighting gives a general strategy to calculate expectation values in a target theory - with path integral weights $w_t(U)$ and partition function $Z_t = \int \mathcal{D}U w_t(U)$ - by performing simulations in a different (simulated) theory - with path integral weights $w_s(U)$ and partition function $Z_s = \int \mathcal{D}U w_s(U)$. The ratio of the partition functions and expectation value in the target theory are given by the following formulas:

$$Z_t/Z_s = \langle w_t/w_s \rangle_s \quad \text{and} \quad \langle O \rangle_t = \langle O w_t/w_s \rangle_s / \langle w_t/w_s \rangle_s \tag{13}$$

where $\langle \dots \rangle_{t,s}$ denotes taking expectation value with respect to the weights in the tartget and simulated theories respectively. Since in our case the target theory is lattice QCD at $\mu_B > 0$, the weights $w_t(U)$ have wildly fluctuating phases: this is the sign problem. In addition to this problem, generic reweighting methods also suffer from an overlap problem: the probability density function of the reweighting factors w_t/w_s has generally a long tail, which cannot be sampled efficiently with standard Monte Carlo methods. This overlap problem in the weights w_t/w_s is not present if they take values in some compact space. For simplicity,let us consider the case

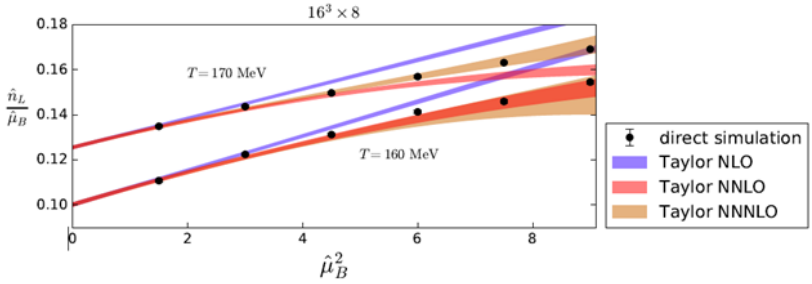

Figure 7: Direct results (black points) versus different orders of the Taylor expansion (colored bands) for the density-to-chemical potential ratio as a function of $\hat{\mu}_B^2 = (\mu_B/T)^2$ for two different temperatures.

when only the u and d quarks have a non-zero chemical potential $\mu = \mu_u = \mu_d$. The most well-known approach without an overlap problem in w_t/w_s is phase reweighting [69], where $w_s = w_{PQ} = |\det M_u(\mu_u = \mu_B/3) \det M_d(\mu_d = \mu_B/3)| \det M_s(\mu_s = 0) e^{-S_{YM}}$. In this case the reweighting factors are pure phases: $(w_t/w_s)_{PQ} = e^{i\theta}$, where $\theta = \mathrm{Arg}\,(\det M_u \det M_d)$. An other approach is sign reweighting [62, 70–72], where $w_s = w_{SQ} = |\,\mathrm{Re} \det M_u(\mu_u = \mu_B/3) \det M_d(\mu_d = \mu_B/3)| \det M_s(\mu_s = 0) e^{-S_{YM}}$. In this case the reweighting factors are signs $(w_t/w_s)_{SQ} = \epsilon \equiv \mathrm{sign} \cos\theta = \pm 1$. Here I suppressed details of the discretization, including staggered rooting, when present. For details on implementing these schemes in lattice QCD see Refs. [62, 72, 73]. The severity of the sign problem can be quantified via the expectation value of the phases or signs respectively. Details on the severity of the sign problem can be found in Refs. [53, 62].

Recent technical advances have made it possible to use both of these schemes for physics applications. E.g., in Ref. [62] it was shown that the existence of an approximate scaling variable, originally demonstrated with imaginary chemical potential simulations, can also be demonstrated on data gathered directly at a real chemical potential. An other example is shown in Fig. 7, where different orders of the Taylor expansion are compared with direct simulations for the density-to-chemical potential ratio. At fourth order, the Taylor expansion gives accurate results for about $\mu_B/T < 2$. Going to eigths order extends this range up to at least $\mu_B/T = 3$. Alternatively, one can use only the fourth order Taylor coefficients to calculate the κ_2 coefficient of the resummation scheme defined in eq. 12 to also get an accurate equation of state up to up to at least $\mu_B/T = 3$. Thus, the resummation scheme based on shifting sigmoid functions demonstrates much faster convergence.

An interesting technical detail in reweighting calculations is that rooted staggered fermions (which are the most common discretization in QCD thermodynamics) introduce cut-off effects that are non-analytic in the chemical potential [58, 74, 75]. Numerical evidence in Ref. [75] points to an essential singularity at $\mu_B = 0$. This makes it hard to use staggered fermions to study small T and large μ_B with more direct methods. This makes it desirable to study other discretizations, that retain the cost-effectiveness of staggered fermions for QCD thermodynamics, but involve no rooting. Minimally doubled fermions [76–80], e.g., could be an interesting alternative for this use-case.

4. Summary and outlook

I have discussed lattice QCD calculations of the QCD phase diagram. While we have learnt a lot over the years, there are two questions that remain unsolved:

1. What happens to the chiral transition in the chiral limit?
2. What happens to the chiral transition at large baryochemical potentials μ_B?

The two questions are related. Thus, the second (phenomenologically very relevant question) also gives extra motivation to study the first (more theoretical) question. Significant progress on the first question probably requires developments in simulations with chirally symmetric fermions on the lattice. There is also an interesting open statistical field theory question about whether there is a new universality class for the $N_f = 3$ chiral limit, or the standard lore of there being no renormalization group fixed point for the correponsing symmetry breaking pattern is correct.

Due to the sign problem, the second question is currently mostly studied with analytic continuation methods. Current lattice results are available in a range of baryochemical potentials that roughly overlaps with the experimental range of the RHIC Beam Energy Scan. Thus, in spite of the difficulty of the sign problem, first-priciples theory has mostly managed to keep up with the experimental effort. This is in part due to an increase in the available computational resources, and in part due to the invention of new extrapolation techniques, such as the alternative expansion scheme/resummation of Refs. [10, 61]. Continuum extrapolated lattice QCD results lead to a rather consistent picture: a crossover transition with a temperature that is μ_B dependent, but with a width that is approximately constant in μ_B for at least most of the range of the RHIC Beam Energy Scan. While the state-of-the-art lattice results do reach the end of the RHIC range in collider mode, at the largest densities, the errorbars start to increase. E.g., while there is no sign of critical lensing in Fig. 6, the current error bars do allow for some of it for the largest densities reached at RHIC in collider mode. Thus, results from phase II of the RHIC Beam Energy Scan should be interesting, as they will shed some light on the position of the coveted critical endpoint. For theory to also keep up with future experiments, where considerably larger densities will be studied, theoretical/calculational innovations will be necessary. Such developments will be a priority for the lattice QCD community in the coming years. One avenue for the development for novel methods is the development of different resummation schemes for the Taylor expansion. I discussed schemes based on shifting sigmoid functions in more detail [10, 61, 62]. Other avenues include the use of Padé approximants [36, 59, 60] and truncated approximations of reweighting [81, 82]. More direct reweighting methods are an other avenue that deserves further work, since they completely do away with the need for an analytic continuation. They will become especially powerful, if reweighting in QCD can be later combined with ideas on mitigating the sign problem itselfm, such as complex deformations of the integration manifold of the path integral [83–89].

Acknowledgements

This research was supported by the Hungarian National Research, Development and Innovation Office, NKFIH Grant No. KKP126769 and by the NKFIH excellence grant TKP2021_NKTA_64 and under Project No. FK 147164.

References

[1] Y. Aoki et al. The Order of the quantum chromodynamics transition predicted by the standard model of particle physics. *Nature*, 443:675–678, 2006.

[2] Peter Kovács, Zsolt Szép, and György Wolf. Existence of the critical endpoint in the vector meson extended linear sigma model. *Phys. Rev. D*, 93(11):114014, 2016.

[3] Philipp Isserstedt et al. Baryon number fluctuations in the QCD phase diagram from Dyson-Schwinger equations. *Phys. Rev. D*, 100(7):074011, 2019.

[4] Wei-jie Fu et al. Hyper-order baryon number fluctuations at finite temperature and density. *Phys. Rev. D*, 104(9):094047, 2021.

[5] Philippe de Forcrand. Simulating QCD at finite density. *PoS*, LAT2009:010, 2009.

[6] B. B. Brandt, G. Endrodi, and S. Schmalzbauer. QCD phase diagram for nonzero isospin-asymmetry. *Phys. Rev. D*, 97(5):054514, 2018.

[7] G. S. Bali, F. Bruckmann, G. Endrodi, Z. Fodor, S. D. Katz, S. Krieg, A. Schafer, and K. K. Szabo. The QCD phase diagram for external magnetic fields. *JHEP*, 02:044, 2012.

[8] Massimo D'Elia, Lorenzo Maio, Francesco Sanfilippo, and Alfredo Stanzione. Phase diagram of QCD in a magnetic background. *Phys. Rev. D*, 105(3):034511, 2022.

[9] Paolo Alba et al. Constraining the hadronic spectrum through QCD thermodynamics on the lattice. *Phys. Rev. D*, 96(3):034517, 2017.

[10] Szabolcs Borsányi et al. Resummed lattice QCD equation of state at finite baryon density: Strangeness neutrality and beyond. *Phys. Rev. D*, 105(11):114504, 2022.

[11] Francesca Cuteri, Owe Philipsen, and Alessandro Sciarra. On the order of the QCD chiral phase transition for different numbers of quark flavours. *JHEP*, 11:141, 2021.

[12] G. Boyd, J. Engels, F. Karsch, E. Laermann, C. Legeland, M. Lutgemeier, and B. Petersson. Thermodynamics of SU(3) lattice gauge theory. *Nucl. Phys. B*, 469:419–444, 1996.

[13] Kieran Holland and Uwe-Jens Wiese. The Center symmetry and its spontaneous breakdown at high temperatures. pages 1909–1944, 11 2000.

[14] Szabolcs Borsanyi, Zoltan Fodor, Jana N. Guenther, Ruben Kara, Paolo Parotto, Attila Pasztor, and Denes Sexty. The upper right corner of the Columbia plot with staggered fermions. *PoS*, LATTICE2021:496, 2022.

[15] Robert D. Pisarski and Frank Wilczek. Remarks on the Chiral Phase Transition in Chromodynamics. *Phys. Rev. D*, 29:338–341, 1984.

[16] Agostino Butti, Andrea Pelissetto, and Ettore Vicari. On the nature of the finite temperature transition in QCD. *JHEP*, 08:029, 2003.

[17] G. Fejos. Second-order chiral phase transition in three-flavor quantum chromodynamics? *Phys. Rev. D*, 105(7):L071506, 2022.

[18] H. T. Ding et al. Chiral Phase Transition Temperature in (2+1)-Flavor QCD. *Phys. Rev. Lett.*, 123(6):062002, 2019.

[19] Andrey Yu. Kotov, Maria Paola Lombardo, and Anton Trunin. QCD transition at the physical point, and its scaling window from twisted mass Wilson fermions. *Phys. Lett. B*, 823:136749, 2021.

[20] Yu Zhang, Yasumichi Aoki, Shoji Hashimoto, Issaku Kanamori, Takashi Kaneko, and Yoshifumi Nakamura. Finite temperature QCD phase transition with 3 flavors of Mobius domain wall fermions. *PoS*, LATTICE2022:197, 2023.

[21] Lorenzo Dini, Prasad Hegde, Frithjof Karsch, Anirban Lahiri, Christian Schmidt, and Sipaz Sharma. Chiral phase transition in three-flavor QCD from lattice QCD. *Phys. Rev. D*, 105(3):034510, 2022.

[22] Julian Bernhardt and Christian S. Fischer. QCD phase transitions in the light quark chiral limit. *Phys. Rev. D*, 108(11):114018, 2023.

[23] Sinya Aoki, Hidenori Fukaya, and Yusuke Taniguchi. Chiral symmetry restoration, eigenvalue density of Dirac operator and axial U(1) anomaly at finite temperature. *Phys. Rev. D*, 86:114512, 2012.

[24] Robert G. Edwards, Urs M. Heller, Joe E. Kiskis, and Rajamani Narayanan. Chiral condensate in the deconfined phase of quenched gauge theories. *Phys. Rev. D*, 61:074504, 2000.

[25] Olaf Kaczmarek, Lukas Mazur, and Sayantan Sharma. Eigenvalue spectra of QCD and the fate of UA(1) breaking towards the chiral limit. *Phys. Rev. D*, 104(9):094518, 2021.

[26] Andrei Alexandru and Ivan Horváth. Possible New Phase of Thermal QCD. *Phys. Rev. D*, 100(9):094507, 2019.

[27] Andrei Alexandru and Ivan Horváth. Unusual Features of QCD Low-Energy Modes in the Infrared Phase. *Phys. Rev. Lett.*, 127(5):052303, 2021.

[28] H. T. Ding, S. T. Li, Swagato Mukherjee, A. Tomiya, X. D. Wang, and Y. Zhang. Correlated Dirac Eigenvalues and Axial Anomaly in Chiral Symmetric QCD. *Phys. Rev. Lett.*, 126(8):082001, 2021.

[29] S. Aoki, Y. Aoki, G. Cossu, H. Fukaya, S. Hashimoto, T. Kaneko, C. Rohrhofer, and K. Suzuki. Study of the axial $U(1)$ anomaly at high temperature with lattice chiral fermions. *Phys. Rev. D*, 103(7):074506, 2021.

[30] Tamas G. Kovacs. The fate of chiral symmetries in the quark-gluon plasma. 11 2023.

[31] A. Bazavov et al. The QCD Equation of State to $O(\mu_B^6)$ from Lattice QCD. *Phys. Rev. D*, 95(5):054504, 2017.

[32] C. R. Allton, S. Ejiri, S. J. Hands, O. Kaczmarek, F. Karsch, E. Laermann, C. Schmidt, and L. Scorzato. The QCD thermal phase transition in the presence of a small chemical potential. *Phys. Rev.*, D66:074507, 2002.

[33] Szabolcs Borsányi et al. Is there still any T_c mystery in lattice QCD? Results with physical masses in the continuum limit III. *JHEP*, 09:073, 2010.

[34] A. Bazavov et al. Polyakov loop in 2+1 flavor QCD from low to high temperatures. *Phys. Rev. D*, 93(11):114502, 2016.

[35] Szabolcs Borsanyi et al. QCD Crossover at Finite Chemical Potential from Lattice Simulations. *Phys. Rev. Lett.*, 125(5):052001, 2020.

[36] Attila Pásztor, Zsolt Szép, and Gergely Markó. Apparent convergence of Padé approximants for the crossover line in finite density QCD. *Phys. Rev. D*, 103(3):034511, 2021.

[37] Claudio Bonati et al. Curvature of the chiral pseudocritical line in QCD: Continuum extrapolated results. *Phys. Rev. D*, 92(5):054503, 2015.

[38] R. Bellwied et al. The QCD phase diagram from analytic continuation. *Phys. Lett.*, B751:559–564, 2015.

[39] Claudio Bonati et al. Curvature of the pseudocritical line in QCD: Taylor expansion matches analytic continuation. *Phys. Rev.*, D98(5):054510, 2018.

[40] A. Bazavov et al. Chiral crossover in QCD at zero and non-zero chemical potentials. *Phys. Lett. B*, 795:15–21, 2019.

[41] P. Braun-Munzinger et al. Chemical freezeout and the QCD phase transition temperature. *Phys. Lett. B*, 596:61–69, 2004.

[42] Anton Andronic et al. Decoding the phase structure of QCD via particle production at high energy. *Nature*, 561(7723):321–330, 2018.

[43] Anton Andronic et al. The thermal proton yield anomaly in Pb-Pb collisions at the LHC and its resolution. *Phys. Lett. B*, 792:304–309, 2019.

[44] Fernando Antonio Flor, Gabrielle Olinger, and Rene Bellwied. Flavour and Energy Dependence of Chemical Freeze-out Temperatures in Relativistic Heavy Ion Collisions from RHIC-BES to LHC Energies. *Phys. Lett. B*, 814:136098, 2021.

[45] Fernando Antonio Flor, Gabrielle Olinger, and René Bellwied. System size and flavour dependence of chemical freeze-out temperatures in ALICE data from pp, pPb and PbPb collisions at LHC energies. *Phys. Lett. B*, 834:137473, 2022.

[46] Stefan Floerchinger and Christof Wetterich. Chemical freeze-out in heavy ion collisions at large baryon densities. *Nucl. Phys. A*, 890-891:11–24, 2012.

[47] Roger Dashen, Shang-Keng Ma, and Herbert J. Bernstein. S Matrix formulation of statistical mechanics. *Phys. Rev.*, 187:345–370, 1969.

[48] R. Venugopalan and M. Prakash. Thermal properties of interacting hadrons. *Nucl. Phys. A*, 546:718–760, 1992.

[49] Massimo D'Elia, Giuseppe Gagliardi, and Francesco Sanfilippo. Higher order quark number fluctuations via imaginary chemical potentials in $N_f = 2+1$ QCD. *Phys. Rev. D*, 95(9):094503, 2017.

[50] Szabolcs Borsányi et al. Higher order fluctuations and correlations of conserved charges from lattice QCD. *JHEP*, 10:205, 2018.

[51] A. Bazavov et al. Skewness, kurtosis, and the fifth and sixth order cumulants of net baryon-number distributions from lattice QCD confront high-statistics STAR data. *Phys. Rev. D*, 101(7):074502, 2020.

[52] D. Bollweg et al. Taylor expansions and Padé approximants for cumulants of conserved charge fluctuations at nonvanishing chemical potentials. *Phys. Rev. D*, 105(7):074511, 2022.

[53] Szabolcs Borsányi et al. Continuum extrapolated high order baryon fluctuations. 12 2023.

[54] E. Follana, Q. Mason, C. Davies, K. Hornbostel, G. P. Lepage, J. Shigemitsu, H. Trottier, and K. Wong. Highly improved staggered quarks on the lattice, with applications to charm physics. *Phys. Rev. D*, 75:054502, 2007.

[55] R. Bellwied, S. Borsányi, Z. Fodor, S. D. Katz, A. Pásztor, C. Ratti, and K. K. Szabó. Fluctuations and correlations in high temperature QCD. *Phys. Rev.*, D92(11):114505, 2015.

[56] P. Hasenfratz and F. Karsch. Chemical Potential on the Lattice. *Phys. Lett. B*, 125:308–310, 1983.

[57] Matteo Giordano and Attila Pásztor. Reliable estimation of the radius of convergence in finite density QCD. *Phys. Rev. D*, 99(11):114510, 2019.

[58] Matteo Giordano et al. Radius of convergence in lattice QCD at finite μ_B with rooted staggered fermions. *Phys. Rev. D*, 101(7):074511, 2020.

[59] P. Dimopoulos et al. Contribution to understanding the phase structure of strong interaction matter: Lee-Yang edge singularities from lattice QCD. *Phys. Rev. D*, 105(3):034513, 2022.

[60] Gokce Basar. On the QCD critical point, Lee-Yang edge singularities and Pade resummations. 12 2023.

[61] Sz. Borsányi et al. Lattice QCD equation of state at finite chemical potential from an alternative expansion scheme. *Phys. Rev. Lett.*, 126(23):232001, 2021.

[62] Szabolcs Borsanyi et al. Lattice simulations of the QCD chiral transition at real baryon density. *Phys. Rev. D*, 105(5):L051506, 2022.

[63] Chiho Nonaka and Masayuki Asakawa. Hydrodynamical evolution near the QCD critical end point. *Phys. Rev. C*, 71:044904, 2005.

[64] Travis Dore et al. Critical lensing and kurtosis near a critical point in the QCD phase diagram in and out of equilibrium. *Phys. Rev. D*, 106(9):094024, 2022.

[65] D. Bollweg, D. A. Clarke, J. Goswami, O. Kaczmarek, F. Karsch, Swagato Mukherjee, P. Petreczky, C. Schmidt, and Sipaz Sharma. Equation of state and speed of sound of (2+1)-flavor QCD in strangeness-neutral matter at nonvanishing net baryon-number density. *Phys. Rev. D*, 108(1):014510, 2023.

[66] L. Adamczyk et al. Bulk Properties of the Medium Produced in Relativistic Heavy-Ion Collisions from the Beam Energy Scan Program. *Phys. Rev. C*, 96(4):044904, 2017.

[67] J. Adam et al. Nonmonotonic Energy Dependence of Net-Proton Number Fluctuations. *Phys. Rev. Lett.*, 126(9):092301, 2021.

[68] Micheal Kahangirwe, Steffen A. Bass, Johannes Jahan, Pierre Moreau, Paolo Parotto, Claudia Ratti, Olga Soloveva, Misha Stephanov, and Elena Bratkovskaya. Lattice-based equation of state with 3D Ising critical point. 12 2023.

[69] Zoltan Fodor, Sandor D. Katz, and Christian Schmidt. The Density of states method at non-zero chemical potential. *JHEP*, 03:121, 2007.

[70] P. de Forcrand, S. Kim, and T. Takaishi. QCD simulations at small chemical potential. *Nucl. Phys. B Proc. Suppl.*, 119:541–543, 2003.

[71] Andrei Alexandru, Manfried Faber, Ivan Horvath, and Keh-Fei Liu. Lattice QCD at finite density via a new canonical approach. *Phys. Rev. D*, 72:114513, 2005.

[72] Matteo Giordano, Kornel Kapas, Sandor D. Katz, Daniel Nogradi, and Attila Pasztor. New approach to lattice QCD at finite density; results for the critical end point on coarse lattices. *JHEP*, 05:088, 2020.

[73] Szabolcs Borsányi et al. Equation of state of a hot-and-dense quark gluon plasma: Lattice simulations at real μB vs extrapolations. *Phys. Rev. D*, 107(9):L091503, 2023.

[74] Maarten Golterman, Yigal Shamir, and Benjamin Svetitsky. Breakdown of staggered fermions at nonzero chemical potential. *Phys. Rev. D*, 74:071501, 2006.

[75] Szabolcs Borsanyi, Zoltan Fodor, Matteo Giordano, Jana N. Guenther, Sandor D. Katz, Attila Pasztor, and Chik Him Wong. Can rooted staggered fermions describe nonzero baryon density at low temperatures? 8 2023.

[76] Luuk H. Karsten. Lattice Fermions in Euclidean Space-time. *Phys. Lett. B*, 104:315–319, 1981.

[77] Frank Wilczek. ON LATTICE FERMIONS. *Phys. Rev. Lett.*, 59:2397, 1987.

[78] Stefano Capitani, Johannes Weber, and Hartmut Wittig. Minimally doubled fermions at one loop. *Phys. Lett. B*, 681:105–112, 2009.

[79] Stefano Capitani, Michael Creutz, Johannes Weber, and Hartmut Wittig. Renormalization of minimally doubled fermions. *JHEP*, 09:027, 2010.

[80] Stefano Capitani, Michael Creutz, Johannes Weber, and Hartmut Wittig. Minimally doubled fermions and their renormalization. *PoS*, LATTICE2010:093, 2010.

[81] Sourav Mondal, Swagato Mukherjee, and Prasad Hegde. Lattice QCD Equation of State for Nonvanishing Chemical Potential by Resumming Taylor Expansions. *Phys. Rev. Lett.*, 128(2):022001, 2022.

[82] Sabarnya Mitra, Prasad Hegde, and Christian Schmidt. New way to resum the lattice QCD Taylor series equation of state at finite chemical potential. *Phys. Rev. D*, 106(3):034504, 2022.

[83] Marco Cristoforetti, Francesco Di Renzo, and Luigi Scorzato. New approach to the sign problem in quantum field theories: High density QCD on a Lefschetz thimble. *Phys. Rev. D*, 86:074506, 2012.

[84] Andrei Alexandru, Gokce Basar, Paulo F. Bedaque, Gregory W. Ridgway, and Neill C. Warrington. Sign problem and Monte Carlo calculations beyond Lefschetz thimbles. *JHEP*, 05:053, 2016.

[85] Yuto Mori, Kouji Kashiwa, and Akira Ohnishi. Path optimization in 0 + 1D QCD at finite density. *PTEP*, 2019(11):113B01, 2019.

[86] Andrei Alexandru, Gokce Basar, Paulo F. Bedaque, and Neill C. Warrington. Complex paths around the sign problem. *Rev. Mod. Phys.*, 94(1):015006, 2022.

[87] Matteo Giordano, Kornel Kapas, Sandor D. Katz, Attila Pasztor, and Zoltan Tulipant. Exponential improvement of the sign problem via contour deformations in the 2+1D XY model at non-zero density. *Phys. Rev. D*, 106(5):054512, 2022.

[88] Matteo Giordano, Attila Pasztor, David Pesznyak, and Zoltan Tulipant. Alleviating the sign problem in a chiral random matrix model with contour deformations. *Phys. Rev. D*, 108(9):094507, 2023.

[89] Gokce Basar and Joseph Marincel. Heavy-dense QCD, sign optimization and Lefschetz thimbles. 11 2023.